JCTC Journal of Chemical Theory and Computation

Article

pubs.acs.org/JCTC

# Boranil and Related NBO Dyes: Insights From Theory

Siwar Chibani,[†] Azzam Charaf-Eddin,[†] Boris Le Guennic,*[,‡] and Denis Jacquemin*[,†,§]

[†]Laboratoire CEISAM, UMR CNR 6230, Université de Nantes, 2 Rue de la Houssinière, BP 92208, 44322 Nantes Cedex 3, France

[‡]Institut des Sciences Chimiques de Rennes, CNRS, Université de Rennes 1, 1 Av. du General Leclerc, 35042 Rennes Cedex, France

[§]Institut Universitaire de France, 103, bd Saint-Michel, F-75005 Paris Cedex 05, France

Supporting Information

**ABSTRACT:** The simulations of excited-state properties, that is, the 0−0 energies and vibronic shapes, of a large panel of fluorophores presenting a NBO atomic sequence have been achieved with a Time-Dependent Density Functional Theory (TD-DFT) approach. We have combined eight hybrid exchange-correlation functionals (B3LYP, PBE0, M06, BMK, M06-2X, CAM-B3LYP, ωB97X-D, and ωB97) to the linear-response (LR) and the state specific (SS) Polarizable Continuum Model (PCM) methods in both their equilibrium (eq) and nonequilibrium (neq) limits. We show that the combination of the SS-PCM scheme to a functional incorporating a low amount of exact exchange can yield unphysical values for molecules presenting large increase of their dipole moments upon excitation. We therefore apply a functional possessing a large exact exchange ratio to simulate the properties of NBO dyes, including large dyads.

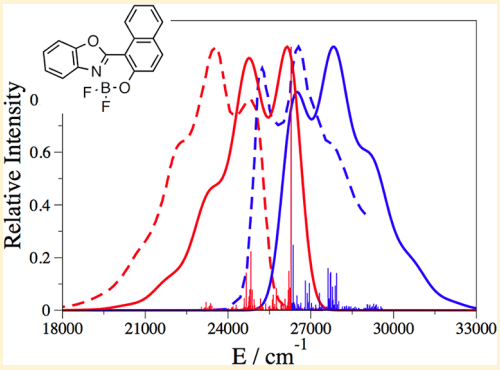


## 1. INTRODUCTION

Organic luminophores recently attracted a widespread interest in several lines of research due to their exciting potential applications. Indeed, these dyes have been used as photosensitizers,[1] laser dyes, filters,[2,3] as well as chemosensors.[4] Among the most important chromophoric classes, boron-dipyrromethene (BODIPY), and aza-boron-dipyrromethene (aza-BODIPY) families (see Scheme 1) have probably been

**Scheme 1. Representation of the Cores (from Left to Right) of BODIPY, aza-BODIPY, Boranil, and HBO complex**

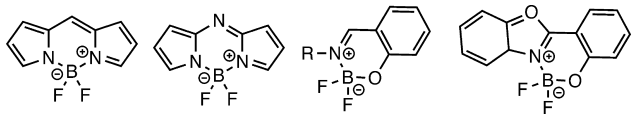

the subject of the largest number of investigations due to their exceptional properties: photostability, near-IR (NIR) emission, large absorption coefficients, and important fluorescent quantum yields.[3,5] However, BODIPY derivatives suffer from several disadvantages, such as generally small Stokes shifts and the practical difficulty of producing industrial quantities. Therefore, a highly desired goal is to increase the Stokes shifts while conserving the other interesting qualities of BODIPY.[6] For this reason, recent efforts have been made to develop new fluoroborate structures presenting features correcting some of the weaknesses of BODIPY dyes.[7−24] For instance, Ziessel and co-workers have synthesized new boron complexes, named boranil (see Scheme 1).[19,23] These compounds, based on the NBO atomic sequence, can be synthesized in two steps. The first implies the reaction between aldehydes and anilines in refluxing ethanol so to reach the *anil*, whereas the second step forms the boranil dyes through the reaction of these *anil* with $BF_3{\cdot}Et_2O$ in the presence of diisopropylethylamine.[19,23] Besides boranil derivatives, other dyes with the NBO pattern have been proposed, such as the 2-(2′-hydroxyphenyl) benzoxazole (HBO) borate complexes (see Scheme 1).[22,25,26] Ziessel et al. and Qian et al. independently investigated several NBO fluorophores of this latter class that present large Stokes shifts as a result of the significant charger-transfer (CT) character of the main electronic transitions.[15,22] Members of the NBO family typically absorb (emit) from 342 (395) nm to 456 (597) nm (see Schemes 2 and 3 for selected examples). To the best of our knowledge, only three previous theoretical works have appeared for NBO structures,[16,27,28] and all relied on Time-Dependent Density Functional Theory (TD-DFT),[29] which is one of the most effective tool for simulating the optical spectra of organic molecules.[30,31] In the first study,[16] Bakalova and co-workers used the vertical TD-DFT approximation for four NBO dyes,[32] whereas in the second work,[27] an adiabatic TD-DFT simulation of four other structures was performed by us in the framework of a more general BODIPY investigation. In the third paper, a limited series of large HBO structures dominated by strong CT transitions were analyzed with a range-separated hybrid (RSH) to explain several unexpected experimental outcomes.[28] Therefore, there was no previous investigation of boranil derivatives nor methodological assessment, nor simulations of an extended series of NBO dyes.

**Received:** May 14, 2013

   dx.doi.org/10.1021/ct400392r | J. Chem. Theory Comput. XXXX, XXX, XXX−XXX

**Scheme 2. Representation of the Systems Used in the Benchmark Step**[a]

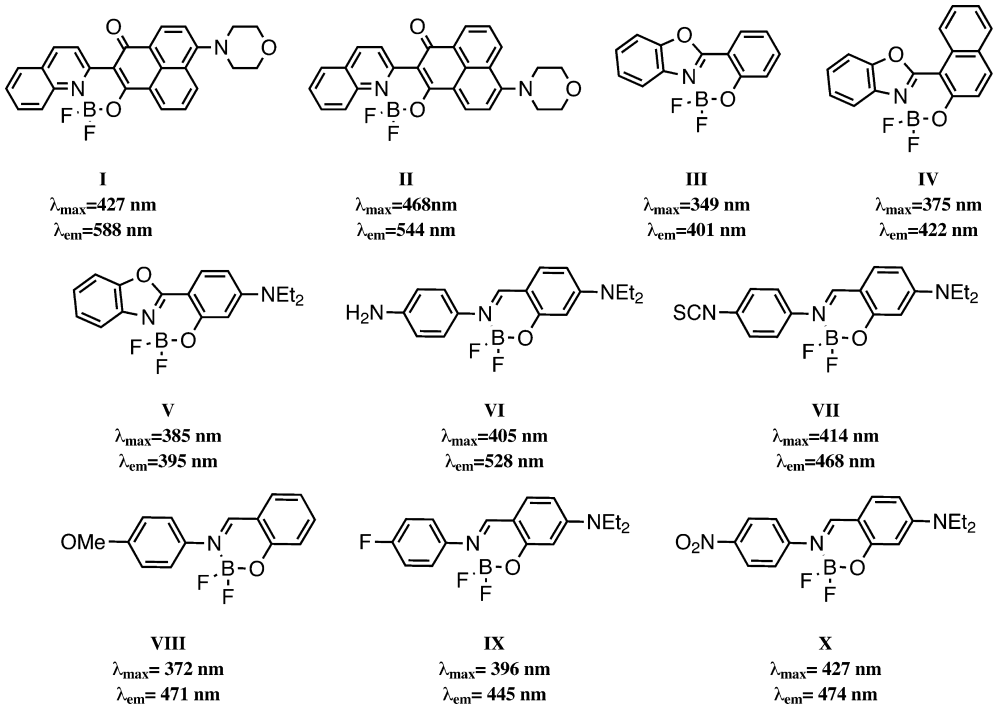


[a]Solvents used as well as experimental references can be found in Table S-I in the Supporting Information (SI).

In the present study, a large panel of boranil as well as other NBO dyes (see Schemes 2 and 3)[15,19,22,23,33,34] presenting CT or cyanine-like transitions are investigated. In this framework, the properties of the excited-states need to be tackled with an efficient yet accurate tool and it is well-known that TD-DFT relying on standard global hybrids may be unsuccessful for both types of electronic transitions.[35] Indeed, CT energies are often strongly underestimated by these hybrids especially when there is a large distance separating the regions gaining/loosing electron density.[36,37] In addition, while most TD-DFT applications published to date have been performed using the vertical TD-DFT scheme, it has been shown that this approximation is not pertinent for cyanine-like transitions.[38−40]

On this basis, as one of the aims of this study is to gauge the relative accuracy of several theoretical models, we have computed the 0−0 energies including vibrational corrections in order to allow meaningful comparison with experiments. Assessing the importance of the environment is crucial, and we have recently demonstrated that the state-specific (SS) corrections[41] of the Polarizable Continuum Model (PCM) significantly affects the computed transition energies of both BODIPY and aza-BODIPY dyes.[27,42] The SS model allows to account for the change of polarization of the cavity surrounding a dye when one goes from one state to the other and has therefore been advocated for structures having a CT nature.[41] On the contrary, in the linear-response (LR) approach,[43,44] the polarization of the cavity computed for the ground-state is conserved for all states making the approach cost-effective. Both methods are thoroughly tested in the present work.

This paper is divided in three main sections. In the following section, we outline our methodology. Next, we present the key results provided by TD-DFT benchmarks with a dual focus on exchange-correlation functionals and solvent models. In a third stage, we apply our methodology to an extended series of NBO compounds, aiming at gaining chemical insights and understanding the key experimental outcomes.

## 2. METHODS

**2.1. Computational Details.** All computations have been performed with the Gaussian 09 program package,[45] applying default thresholds except for a tighten self-consistent field convergence ($10^{-8}$ to $10^{-10}$ au) and an improved optimization threshold ($10^{-5}$ au on average forces). For each molecule, we have optimized the geometry of both the ground and the first excited-states, as well as computed the vibrational spectra of both states. The same DFT integration grid (*fine* or *ultrafine*) was used for all calculations on a given molecule. Our first goal is to define an efficient TD-DFT protocol to simulate the optical properties of NBO dyes. For this reason, we have tested a wide panel of hybrid exchange-correlation functionals, namely B3LYP,[46,47] PBE0,[48,49] M06,[50] BMK,[51] M06-2X,[50] CAM-B3LYP,[52] ωB97X-D,[53] and ωB97,[54] and the results of these benchmarks are presented below. In a recent work, we have performed an extensive assessment of basis set effects for aza-BODIPY dyes.[42] It was found that the geometrical and vibrational parameters can be determined with a relatively compact atomic basis set, that is 6-31G(d), whereas the transition energies need to be corrected using a more extended basis set, namely 6-311+G(2d,p). Therefore, this strategy was applied here (see the next section). The inclusion of environmental effects is crucial to estimate the electronic transition energies especially for excited-states presenting a strong CT character. Here, three solvents have been employed consistently with experiment (see Table S-1 in the SI): toluene (Tol), dichloromethane (DCM), and acetonitrile (ACN). To quantify solvent effects, several PCM approaches[55] have been applied. As stated in the introduction, we have used both PCM approaches implemented in Gaussian 09, namely LR[43,44] and SS[41] models, applied in both their equilibrium (eq) and


dx.doi.org/10.1021/ct400392r | J. Chem. Theory Comput. XXXX, XXX, XXX−XXX

**Scheme 3. Representation of the Second Series of NBO Systems Investigated**[a]

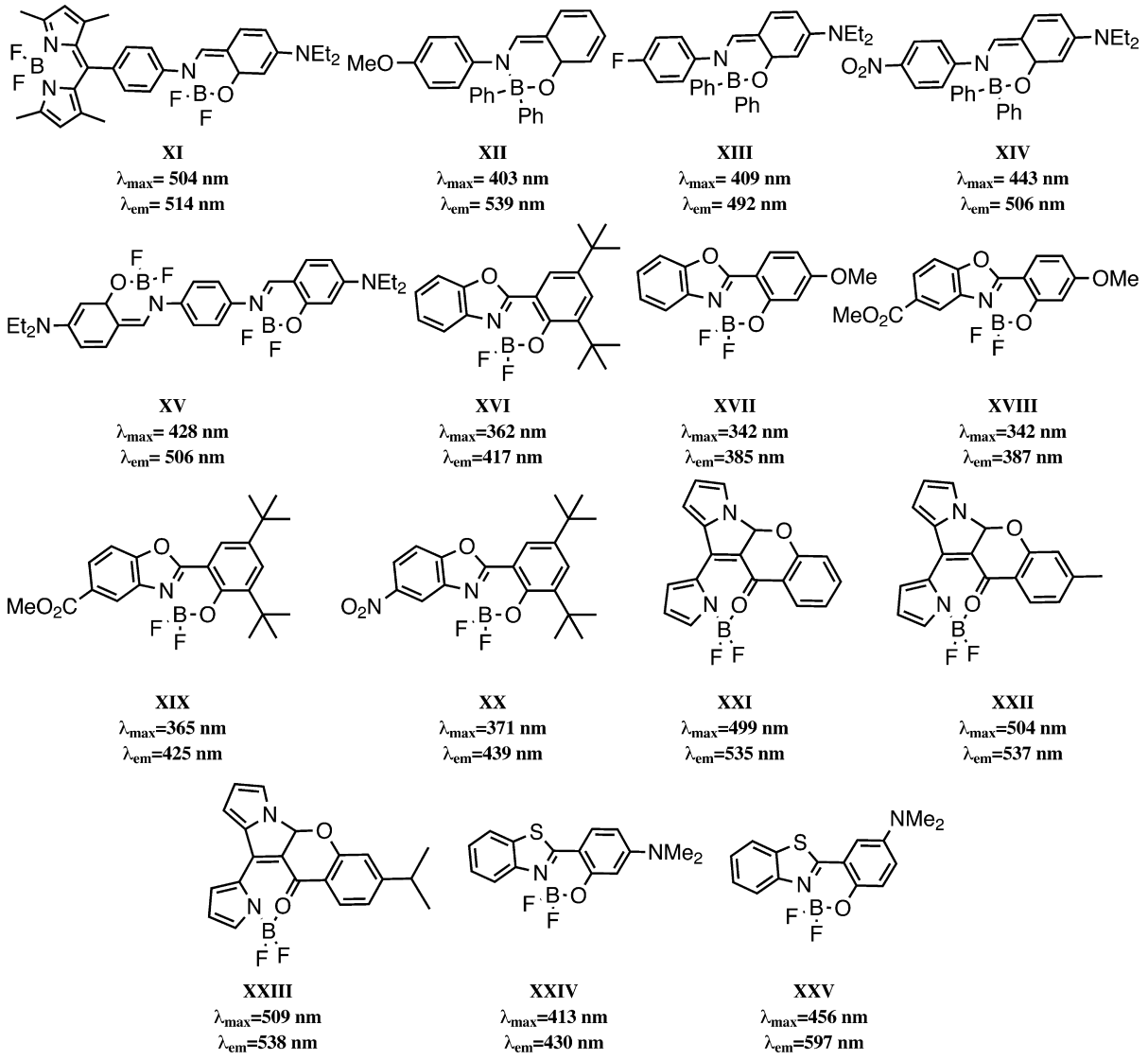


[a]Solvents used and experimental references can be found in Table S−I in the SI.

nonequilibrium (neq) limits.[55] In the neq limit, only the electrons of the solvent do adapt to the new electronic configuration of the solute (fast process). Clearly, the vertical transition energies better correspond to a neq scheme. On the contrary, in the eq approach, the solvent has time to adapt to the new electronic configuration of the solute (slow process). This latter approach is the recommended scheme to calculate excited-states geometries, vibrational signatures, and, consequently, the 0−0 energies.

Vibrationally resolved spectra within the harmonic approximation were computed using the FC classes program (FC).[56−58] The reported spectra have been simulated using a convoluting Gaussian function presenting a half width at half-maximum (HWHM) that has been adjusted to allow meaningful comparisons with experiments (typical value: 0.04 eV). A maximal number of 25 overtones for each mode and 20 combination bands on each pair of modes were included in the calculation. The maximum number of integrals to be computed for each class was set to $10^6$. In the cases where convergence of the FC factors ≥0.9 could not be achieved with this number of integrals, a larger value (up to $10^{12}$) has been used. Note that, in the following, the experimental fluorescence spectra measured in the wavelength scale have been transformed in line shapes by applying an intensity correction proportional to $\omega^2$,[59] as this correction, which allows consistent theory/experiment comparisons, significantly affects the band shapes.[60]

**2.2. Protocols.** The adiabatic energies, $E^{adia}$, are the difference of total electronic energies between the ground-state ($S_0$) and the excited-state ($S_1$) at their respective geometrical minima. In practice, $E^{adia}$ can be estimated in both equilibrium and nonequilibrium, [$X$: eq or neq], using the LR-PCM model:[61]

$$E^{adia}_{6\text{-}31G(d)}(LR, X) = E^{S_1//S_1}_{6\text{-}31G(d)}(LR, X) - E^{S_0//S_0}_{6\text{-}31G(d)}(eq) \quad (1)$$

In order to account for atomic basis set effects, we have determined the adiabatic energies by single point calculations performed with a larger basis set, 6-311+G(2d,p), through eq 1 leading to $E^{adia}_{6\text{-}311+G(2d,p)}$ (LR,X).[62] We have also used the SS model:

$$E^{adia}_{6\text{-}31G(d)}(SS, X) = E^{S_1//S_1}_{6\text{-}31G(d)}(SS, X) - E^{S_0//S_0}_{6\text{-}31G(d)}(eq) \quad (2)$$


dx.doi.org/10.1021/ct400392r | J. Chem. Theory Comput. XXXX, XXX, XXX−XXX

This allows to determine a best estimate (BE) of the adiabatic energies using:

$$E_{BE}^{adia}(SS, X) = E_{6\text{-}31G(d)}^{adia}(SS, X) + [(E_{6\text{-}311+G(2d,p)}^{adia}(LR, X) - E_{6\text{-}31G(d)}^{adia}(LR, X)] \quad (3)$$

We redirect the reader to ref 42 for a longer discussion of this approach. To calculate the $E^{0-0}$ one needs to compute the difference of the zero-point vibrational energy, $\Delta E^{ZPVE}$, between GS and ES,

$$\Delta E_{6\text{-}31G(d)}^{ZPVE}(LR, X) = E_{6\text{-}31G(d)}^{ZPVE-S_1//S_1}(LR, X) - E_{6\text{-}31G(d)}^{ZPVE-S_0//S_0}(eq) \quad (4)$$

The 0−0 energies can now be computed in the LR-PCM approach in both eq and neq limits:

$$E_{BE}^{0-0}(LR, X) = E_{6\text{-}311+G(2d,p)}^{adia}(LR, X) + \Delta E_{6\text{-}31G(d)}^{ZPVE}(LR, X) \quad (5)$$

and the same holds for the SS model:

$$E_{BE}^{0-0}(SS, X) = E_{BE}^{adia}(SS, X) + \Delta E_{6\text{-}31G(d)}^{ZPVE}(LR, X) \quad (6)$$

In addition, the equilibrium 0−0 energies of the eq 6 can also be corrected for nonequilibrium effects in order to compare directly our results to the experimental absorption/fluorescence crossing point (AFCP), the accepted experimental reference of 0−0 energies,[63,64]

$$E_{BE}^{AFCP}(SS, neq) = E_{BE}^{0-0}(SS, eq) + \Delta E_{neq/eq}(SS) \quad (7)$$

where a correction for the neq effects, determined from the vertical absorption/fluorescence energies, has been introduced:

$$\Delta E_{neq/eq}(SS) = \frac{1}{2}[\Delta E_{neq/eq}^{abso}(SS) + \Delta E_{neq/eq}^{fluo}(SS)] \quad (8)$$

We redirect the reader to ref 64 for more details. In this case, we have calculated the $E^{vert-a}$ in both eq and neq limits within the SS-PCM model:

$$E_{6\text{-}31G(d)}^{vert-a}(SS, neq) = E_{6\text{-}31G(d)}^{S_1//S_0}(SS, neq) - E_{6\text{-}31G(d)}^{S_0//S_0}(eq) \quad (9)$$

$$E_{6\text{-}31G(d)}^{vert-a}(SS, eq) = E_{6\text{-}31G(d)}^{S_1//S_0}(SS, eq) - E_{6\text{-}31G(d)}^{S_0//S_0}(eq) \quad (10)$$

So to determine the absorption correction,

$$\Delta E_{neq/eq}^{vert-a}(SS) = E_{6-31G(d)}^{vert-a}(SS, neq) - E_{6\text{-}31G(d)}^{vert-a}(SS, eq) \quad (11)$$

In a similar way,

$$E_{6\text{-}31G(d)}^{vert-f}(SS, neq) = E_{6\text{-}31G(d)}^{S_1//S_1-eq}(SS, eq) - E_{6\text{-}31G(d)}^{S_0//S_1}(neq) \quad (12)$$

$$E_{6\text{-}31G(d)}^{vert-f}(SS, eq) = E_{6\text{-}31G(d)}^{S_1//S_1-eq}(SS, eq) - E_{6\text{-}31G(d)}^{S_0//S_1}(eq) \quad (13)$$

$$\Delta E_{neq/eq}^{vert-f}(SS) = E_{6\text{-}31G(d)}^{vert-f}(SS, neq) - E_{6\text{-}31G(d)}^{vert-f}(SS, eq) \quad (14)$$

## 3. METHODOLOGICAL INVESTIGATION

In order to determine an efficient TD-DFT scheme, we have combined a series of hybrid functionals to the five "solvent" protocols detailed, that is, eq 5 and eq 6 using eq and neq limits, as well as eq 7. To this end, we have used the ten dyes shown in Scheme 2. Results of the statistical analysis are presented in Table 1: mean signed error (MSE), mean absolute error (MAE), standard deviation (SD), as well as the theory/experiment linear correlation coefficient ($R^2$). The computed individual energies are listed in Tables S-II to S-VI in the SI. The results in Table 1 show a marked difference between the LR and SS of PCM approaches. For all selected functionals, we have found that the LR-PCM model, irrespective of the selection of the eq and neq limits, is surprisingly more accurate than the SS-PCM one. Indeed, with the LR-PCM approach, the

**Table 1. Statistical Analysis for the Dyes Shown in Scheme 2 Obtained from Comparison between Experimental and Theoretical 0−0 Energies[a]**

| functional | method | MSE | MAE | SD | $R^2$ |
|---|---|---|---|---|---|
| B3LYP | 0−0 (LR,eq) | −0.104 | 0.153 | 0.116 | 0.937 |
| | 0−0 (LR,neq) | −0.120 | 0.140 | 0.154 | 0.900 |
| | 0−0 (SS,eq) | −0.364 | 0.420 | 0.682 | 0.533 |
| | 0−0 (SS,neq) | −0.555 | 0.610 | 0.872 | 0.713 |
| | AFCP (SS,neq) | −0.228 | 0.394 | 0.649 | 0.372 |
| PBE0 | 0−0 (LR,eq) | −0.013 | 0.080 | 0.090 | 0.972 |
| | 0−0 (LR,neq) | 0.035 | 0.072 | 0.084 | 0.951 |
| | 0−0 (SS,eq) | −0.157 | 0.317 | 0.510 | 0.649 |
| | 0−0 (SS,neq) | −0.170 | 0.327 | 0.523 | 0.660 |
| | AFCP (SS,neq) | −0.027 | 0.337 | 0.462 | 0.457 |
| M06 | 0−0 (LR,eq) | −0.040 | 0.073 | 0.068 | 0.966 |
| | 0−0 (LR,neq) | 0.027 | 0.061 | 0.074 | 0.941 |
| | 0−0 (SS,eq) | −0.272 | 0.353 | 0.506 | 0.513 |
| | 0−0 (SS,neq) | −0.158 | 0.266 | 0.456 | 0.645 |
| | AFCP (SS,neq) | −0.173 | 0.351 | 0.483 | 0.319 |
| BMK | 0−0 (LR,eq) | 0.201 | 0.201 | 0.087 | 0.962 |
| | 0−0 (LR,neq) | 0.254 | 0.254 | 0.086 | 0.929 |
| | 0−0 (SS,eq) | 0.242 | 0.297 | 0.214 | 0.878 |
| | 0−0 (SS,neq) | 0.241 | 0.301 | 0.221 | 0.865 |
| | AFCP (SS,neq) | 0.287 | 0.308 | 0.166 | 0.877 |
| M06-2X | 0−0 (LR,eq) | 0.228 | 0.228 | 0.073 | 0.972 |
| | 0−0 (LR,neq) | 0.282 | 0.282 | 0.055 | 0.966 |
| | 0−0 (SS,eq) | 0.310 | 0.310 | 0.137 | 0.939 |
| | 0−0 (SS,neq) | 0.310 | 0.314 | 0.138 | 0.939 |
| | AFCP (SS,neq) | 0.335 | 0.335 | 0.104 | 0.949 |
| CAM-B3LYP | 0−0 (LR,eq) | 0.263 | 0.263 | 0.062 | 0.965 |
| | 0−0 (LR,neq) | 0.311 | 0.311 | 0.053 | 0.965 |
| | 0−0 (SS,eq) | 0.348 | 0.348 | 0.131 | 0.907 |
| | 0−0 (SS,neq) | 0.342 | 0.342 | 0.137 | 0.905 |
| | AFCP (SS,neq) | 0.376 | 0.376 | 0.106 | 0.907 |
| ωB97X-D | 0−0 (LR,eq) | 0.293 | 0.293 | 0.064 | 0.957 |
| | 0−0 (LR,neq) | 0.343 | 0.343 | 0.064 | 0.950 |
| | 0−0 (SS,eq) | 0.383 | 0.383 | 0.126 | 0.899 |
| | 0−0 (SS,neq) | 0.380 | 0.380 | 0.130 | 0.898 |
| | AFCP (SS,neq) | 0.401 | 0.401 | 0.104 | 0.905 |
| ωB97 | 0−0 (LR,eq) | 0.468 | 0.468 | 0.054 | 0.964 |
| | 0−0 (LR,neq) | 0.519 | 0.519 | 0.062 | 0.958 |
| | 0−0 (SS,eq) | 0.581 | 0.581 | 0.085 | 0.933 |
| | 0−0 (SS,neq) | 0.580 | 0.580 | 0.088 | 0.930 |
| | AFCP (SS,neq) | 0.589 | 0.589 | 0.075 | 0.935 |

[a]MSE, MAE, and SD are in eV.


dx.doi.org/10.1021/ct400392r | J. Chem. Theory Comput. XXXX, XXX, XXX−XXX

$R^2$ present larger values: it ranges from 0.90 (B3LYP) to 0.97 (M06-2X) whereas with the SS model a much smaller $R^2$ (several below 0.70) are often found, especially with the three functionals presenting low exact exchange percentage (that is B3LYP, PBE0, and M06). In the same time, both MSE and MAE systematically increase when going from LR to SS, irrespective of the functional. On the contrary, in recent studies, we have shown that the SS-PCM model is the most efficient tool to simulate the optical properties of both BODIPY and aza-BODIPY dyes.[27,42] To explain this unexpected outcome for NBO structures, we have computed the dipole moments of the ground and excited-states, as the SS correction is closely related to the magnitude of the dipole moments. For **X**, the most polar molecule of this series, the dipole moment of $S_0$ is 13.4 (13.7) D, while in the $S_1$ it increases to reach 20.2 (32.4) D with M06-2X (B3LYP). Dipoles obtained for other functionals can be found in Table S-VII, SI, and it is clear that while the dipoles computed for $S_0$ are similar for all functionals, the magnitude of the ES dipole moment is proportional to the inverse of the exact exchange ratio. For the record, the dipoles have also been determined in acetonitrile (see the SI), a more polar solvent to assess interplay between the dielectric constant and the exact exchange ratio, and it turns out, as could be expected, that the ES-GS dipole difference seems to be problematic for functionals such as BMK that were reasonable in a toluene environment. Therefore, for **X**, the combination of B3LYP, PBE0, or M06 with the SS approach yields to an unphysical (over) polarization of the cavity during the SS self-consistent calculations. This leads to unphysically small 0−0 energies, for example, 0.806 eV with (SS,neq) and the B3LYP functional in toluene. In a similar way, the difference between the eq and neq SS excited-state energies of **X** attains 1.11 eV in acetontrile with BMK, which is clearly a problematic "correction". We have therefore performed a statistical analysis removing **X** from our set (see Table S-VIII, SI), and the SS $R^2$ values significantly improve for the three low-exact exchange functionals. Therefore, though the SS scheme has been shown very efficient for coumarins that also present a sizable increase of dipole moments upon photon absorption,[41] one should be cautious when performing SS calculations on such kind of molecules, especially with "conventional" exchange hybrid functionals. In addition, the differences between the results obtained in the equilibrium and nonequilibrium limits are relatively small in the LR-PCM model, and this is especially true with the bottom four functionals of Table 1. Indeed, the LR,eq-LR,neq $R^2$ discrepancies are 0.037, 0.021, 0.024, 0.033, 0.006, 0.000, 0.007, and 0.006 for B3LYP, PBE0, M06, BMK, M06-2X, CAM-B3LYP, $\omega$B97X-D, and $\omega$B97, respectively. Solvent effects will be discussed in more detail below for an extended set of compounds. Of course, the good behavior of the LR approach could also be partly ascribed to error cancellation. We have therefore performed benchmark in gas phase for the ten molecules using both B3LYP and M06-2X. The obtained $R^2$ values of 0.863 and 0.938, respectively, indicate, on the one hand, that the use of an adequate solvent model improves the consistency of the simulations and, on the other hand, that applying SS model in conjunction with the B3LYP functional is detrimental.

Let us now turn to the impact of the functionals. First, the MSE are negative with B3LYP, PBE0, and M06 hybrid functionals and are positive for the other five functionals, indicating that the theoretical results are underestimated (overestimated) for the former (latter), which is a usual trend for valence excited-states modeled with linear-response TD-DFT.[65] The MAE is small for the three first functionals: it ranges from 0.061 eV (M06) to 0.140 eV (B3LYP) using LR-PCM model in its neq limit and such deviations are small for 0−0 simulations.[63,64] However, this success is at the price of a large SD and a relatively poor $R^2$, at least for B3LYP. At first sight, the M06 (LR,eq) approach could be a very good compromise method: it yields a MAE of 0.073 eV, a SD of 0.068 eV and a $R^2$ of 0.966. However, as stated, the M06 values are very sensitive to the solvent model and strongly degrade if the SS model is applied [$R^2$ of 0.319 with AFCP(SS,neq)], which is clearly not an indication of a robust behavior. The five functionals that include large shares of exact exchange (BMK, M06-2X, CAM-B3LYP, $\omega$B97X-D, and $\omega$B97) are less affected by the solvent model: they provide not only large $R^2$ (0.865−0.972) but also relatively small SD (0.221−0.053 eV), irrespective of the selected PCM approach. From that point of view, one notices that the three top functionals are less satisfying than the bottom five. As stated above, the LR-PCM approach nicely fits experimental trends; we therefore focus on the results obtained with this approach at this stage. The range-separated hybrid $\omega$B97X-D yields the minimal values of $R^2$: 0.957 (LR,eq), 0.950 (LR,neq) whereas the largest SD are obtained with BMK [0.087 (LR,eq), 0.086 (LR,neq)]. Overall, M06-2X, CAM-B3LYP, and $\omega$B97 provide relatively similar statistical data. For the SD ($R^2$), we obtain 0.055 (0.966), 0.053 (0.965), and 0.062 (0.958), for these three functionals with the (LR,neq) model, respectively, and these three functionals could have been chosen. In particular, the results in Table 1 indicate that M06-2X could supply a very good accuracy. It yields the most consistent estimations of all PCM models [$R^2$ reaches 0.972 (LR,eq)]. We underline that M06-2X is one of the most powerful functionals to describe cyanine-like transitions,[40] and was also demonstrated to yield accurate values of the adiabatic energies of BODIPY dyes.[27] Consequently, for the sake of consistency with previous studies, we go for the M06-2X in the following, though other choices such as M06 could have been a reasonable selection as well.

We have just shown that the LR-PCM model in both eq and neq limits provides an interesting consistency with the experiment. To check this conclusion, obtained for a limited number of dyes, we have increased the number of NBO compounds using all boranils and NBO dyes represented in both Schemes 2 and 3. All calculations have been performed with the M06-2X hybrid functional, and the statistical results are presented in Table 2 (raw data can be found in the SI). We note that the LR-PCM model in the eq limit ensures the minimal error of calculations: its MSE and MAE are 0.249 eV, as shown in Table 2. In the SI, the adiabatic energies and the $\Delta E^{ZPVE}$ obtained from LR,eq simulations are listed: the ZPVE

**Table 2. Statistical Analysis for Dyes in Schemes 2 and 3 Obtained from Comparison between Experimental and Theoretical 0−0 Energies[a]**

| method | MSE | MAE | SD | $R^2$ |
|---|---|---|---|---|
| 0−0 (LR,eq) | 0.249 | 0.249 | 0.122 | 0.908 |
| 0−0 (LR,neq) | 0.302 | 0.302 | 0.104 | 0.911 |
| 0−0 (SS,eq) | 0.296 | 0.313 | 0.156 | 0.889 |
| 0−0 (SS,neq) | 0.295 | 0.314 | 0.157 | 0.888 |
| AFCP (SS,neq) | 0.315 | 0.322 | 0.135 | 0.903 |

[a]MSE, MAE, and SD are in eV. All data obtained with M06-2X.


dx.doi.org/10.1021/ct400392r | J. Chem. Theory Comput. XXXX, XXX, XXX−XXX

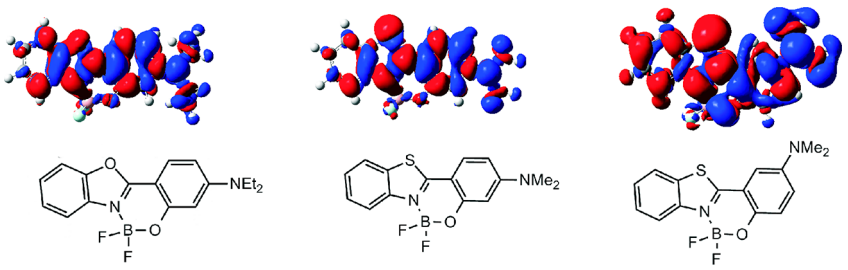


**Figure 1.** PCM-M06-2X/6-31G(d) density difference plots for (from left to right) **V**, **XXIV** and **XXV** (top) and their structures (bottom). The blue (red) zones indicate density decrease (increase) upon transition.

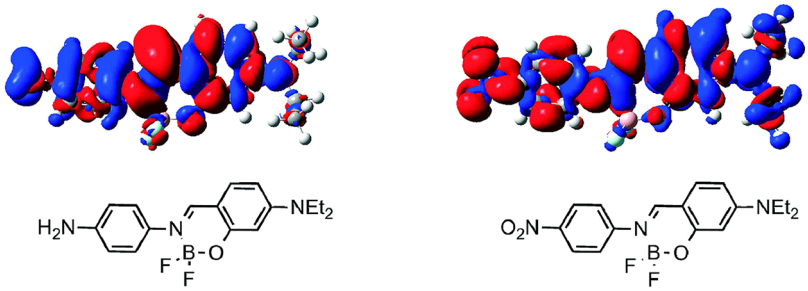


**Figure 2.** PCM-M06-2X/6-31G(d) density difference plots for **VI** (left) and **X** (right).

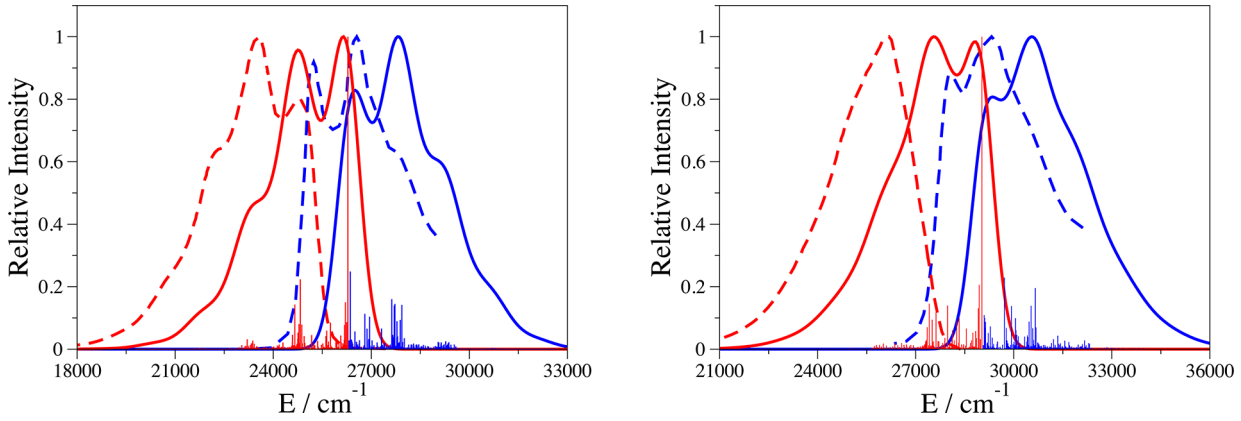


**Figure 3.** Comparison between theoretical (full lines) and experimental (dashed lines) spectra for dyes: (left) **IV** and (right) **XVII**. Absorption and emission spectra are in green and blue, respectively. The experimental spectra are adapted with permission from ref 22. Copyright 2012 American Chemical Society.

correction is in the line of the expected values (−0.06 to −0.12 eV).[35,63,64] One can see from Table 2 that the two SS models in both eq and neq limits also yield consistent estimates but nevertheless provide the largest SD and the smallest $R^2$ of the five PCM model tested (around 0.156 and 0.888, respectively). Clearly, the 0−0(SS) protocols are not the most effective for NBO dyes. The purpose designed AFCP(SS,neq) scheme improves the $R^2$ and SD but still does not outperform the simplest LR approach. The LR-PCM model in neq limit yields the best determination coefficient with 0.911, but the difference with the LR,eq and AFCP schemes is negligible: it does not exceed 0.008. In short, we have selected the LR approach in the equilibrium limit to determine the optical spectra in the following.

## 4. APPLICATIONS

**4.1. Auxochromes' Impact.** Figure 1 gives the M06-2X density difference plots computed for three boranil dyes presenting closely related structures. For **V**, the replacement of the oxygen atom located in position 1 by a sulfur atom to give **XXIV** has a rather small impact. In fact, when going from **V** to **XXIV**, we computed modest bathochromic shifts for both absorption and emission bands: +37 nm and +42 nm, respectively, which is rather close to the experimental values of +28 nm and +35 nm. These limited variations are consistent with the similar topologies of the density difference plots in Figure 1. Using a recently developed approach,[66,67] we have quantified the CT parameters for these dyes. For **V** (**XXIV**), we obtain similar amount of CT charge, 0.49 (0.48) *e*, and alike CT distances of 1.83 (1.99) Å. On the contrary, the last dye, namely **XXV**, presents optical signatures displaced to longer wavelengths compared to both **V** and **XXIV**. Indeed, we found that moving the dimethylamino group from position 9 (**XXIV**) to 10 (**XXV**) induces a sizable bathochromic shift (+42 nm) of the absorption band and an even larger effect for the emission maximum (+107 nm). This outcome can be rationalized in terms of an enhanced CT character: 0.66 *e* being transferred over 2.94 Å (see Figure 1). Concomitantly, the (LR,eq) 0−0


dx.doi.org/10.1021/ct400392r | J. Chem. Theory Comput. XXXX, XXX, XXX−XXX

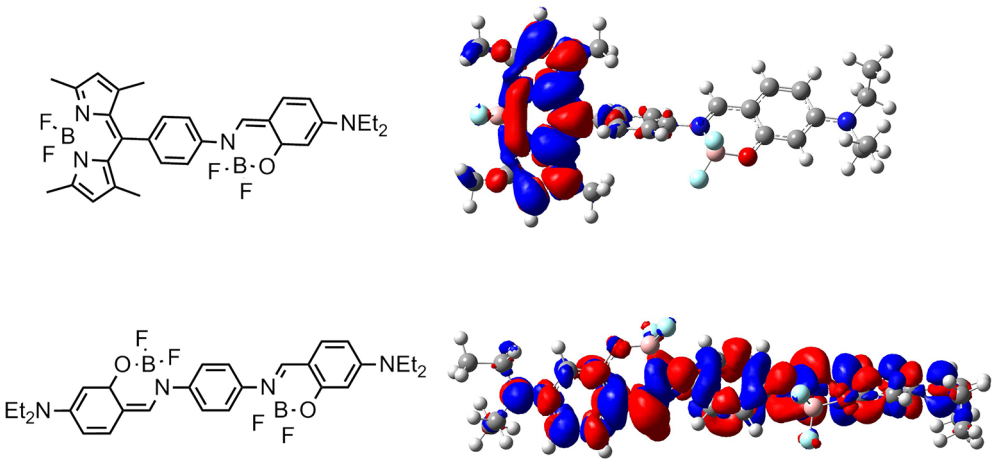

**Figure 4.** PCM-M06-2X/6-31G(d) density difference plots of **XI** (top) and **XV** (bottom).

energy of **XXV** is smaller (2.60 eV) than both its **V** (3.50 eV) and **XXIV** (3.17 eV) counterparts (see Table S-IX in the SI).

We have carried out a similar analysis for **X** and **VI** (more examples can be found in the SI). Comparing **VI** ($\mu^{GS}$= 9.3 D, $\mu^{ES}$= 8.5 D) to **X** ($\mu^{GS}$= 13.3 D, $\mu^{ES}$= 20.1 D), the impact of the replacement of a $NH_2$ group by $NO_2$ is shown to significantly reduce the Stokes shift. Impressively, using the computed vertical values at the M06-2X level, **X** presents a small computed Stokes shift of 46 nm, in line with experiment (47 nm). The much larger Stokes shift predicted for **VI**, (112 nm with M06-2X) also fits experiment (123 nm). This is a valuable success, as the variations of the CT parameters are in the opposite direction, as apparent from the delta density plots of Figure 2. Indeed, the CT distance increases from 0.79 Å to 2.94 Å when going from **VI** to **X**, and this is often thought as inducing larger Stokes shifts. To unravel the origin of this phenomenon, we have investigated the geometries of the GS and ES of both structures. The most notable variation appears for the central C═N double bond that increases by 0.08 Å (0.04 Å) in **VI** (**X**), which is consistent with the Stokes shift ranking. For the records, the computed variation of the position of the emission band when going from **VI** to **X** is −70 nm, which is rather consistent with the measured data of −54 nm.

**4.2. Comparison between Theoretical and Experimental Band Shapes.** The calculation of the vibrational signatures of both $S_0$ and $S_1$ allows determining the shape of the optical spectra of NBO dyes thanks to the calculations of FC factors. In Figure 3, we compare the experimental and theoretical bands of both absorption and emission of **IV** and **XVII**, two of the dyes presenting the most notable vibrational structure. Other vibrationally resolved spectra (**II**, **III**, **V**, **XVI**, **XIX**) obtained through FC calculations are available in the SI. Thanks to the TD-PCM-M06-2X calculations, both the positions and the shapes of all absorption and emission peaks are accurately reproduced (see Figure 3). Indeed, for both **IV** and **XVII**, the crossing point of absorption and fluorescence bands are in agreement with the experiment: 400 (375) and 360 (340) nm for experimental (theoretical), respectively. For **XVII**, the theoretical absorption spectrum presents two important peaks at 1633 $cm^{-1}$ and 686 $cm^{-1}$. These two peaks respectively correspond to the stretching mode of CH and to the breathing of CH, while they do not involve O−C bonds nor the $BF_2$ template (see movies in the SI). For the theoretical emission band of **IV**, the two main vibrational modes explaining the band shape are located at 1455 $cm^{-1}$ and 1623 $cm^{-1}$. These two modes correspond to the stretching mode of the CC and the deformation of the aromatic cycles (see movies in the SI). In addition, for **IV**, the experimental absorption band presents a smaller shoulder at ca. 345 nm. We underline that the height of the shoulder is well reproduced by our computational protocol. The same holds for the emission band, both experimental and theoretical spectra presenting a shoulder at a longer wavelengths (ca. 440 nm).

**4.3. Dyads.** In this section, we characterize two dyads: a BODIPY-boranil compound and a bis-boranil derivative (**XI** and **XV**).[19] The density difference plots corresponding to the first excited-state of these two dyes are displayed in Figure 4. As can be seen, for the first structure, the density is completely located on the BODIPY core, and the boranil group plays no role in the optical transition. This can be explained on the one hand by the orthogonality of the phenyl ring and on the other hand by the fact that BODIPY excited states lie below the ones of boranil. Consistently, in the experiment, the absorption spectra of **XI** is the simple sum of the BODIPY and boranil individual spectra whereas irradiation in the NBO band at 380 nm yields the hallmark emission of BODIPY at 514 nm.[19] For **XV**, the excited-state extends on the two boranil cores and on the phenyl group. As the system is symmetric, the "dipolar" CT distance is zero in spite of the presence of the $NEt_2$ at both extremities.

## 5. CONCLUSIONS

In this work, we have investigated a large panel of members of the NBO fluorophore family. These dyes are characterized by asymmetric cyanine-like transitions, several having also a significant CT character, making the prediction of their optical properties a significant challenge for TD-DFT. For this reason, we have performed a large list of methodological evaluations, and it turned out that there is a significant interplay between the selected solvation model and hybrid functional. On the one hand, we have found that, for structures possessing a strongly increasing dipole moment upon absorption, the state-specific model leads unphysical values when combined to global hybrids incorporating a low amount of exact exchange. In first approximation, it seems possible to detect the problematic cases either by very large LR−SS deviations of the absorption energies, or by very large (SS,neq)−(SS,eq) differences for the transition energies. Consequently, for this specific NBO family, the linear-response PCM model surprisingly outperformed its


dx.doi.org/10.1021/ct400392r | J. Chem. Theory Comput. XXXX, XXX, XXX−XXX

SS counterpart. On the other hand, we found that global hybrids including a large share of exact exchange, or range-separated hybrids provide accurate estimates of auxochromic effects. Using the M06-2X functional, we have simulated several key optical features. It turned out that the proposed method allowed to restore and rationalize: (1) the evolution of the positions of the absorption and emission bands upon substitution; (2) the variation of the Stokes shift in counter-intuitive cases; (3) the band shapes of compounds possessing significant vibronic couplings; and (4) the spectral signatures of symmetric and asymmetric dyads.

## ■ ASSOCIATED CONTENT

### Supporting Information

List of solvent and experimental values. Adiabatic and ZPVE energies for all dyes. Dipole moments of **X**. Extra vibronic analysis and density difference plots. Movies of the key vibrational modes of **IV** and **XVII**. This material is available free of charge via the Internet at http://pubs.acs.org/.

## ■ AUTHOR INFORMATION

### Corresponding Author

*E-mail: Boris.leguennic@univ-rennes1.fr; Denis.Jacquemin@univ-nantes.fr.

### Notes

The authors declare no competing financial interest.

## ■ ACKNOWLEDGMENTS

S.C. and A.C.E. thank the European Research Council (ERC, Marches 278845) for their PhD and postdoctoral grants, respectively. The authors thank G. Ulrich and J. Massue (Laboratoire de Chimie Moléculaire et Spectroscopie Avancées) for fruitful discussions. D.J. acknowledges the European Research Council (ERC) and the Région des Pays de la Loire for financial support in the framework of a Starting Grant (Marches 278845) and a *recrutement sur poste stratégique*, respectively. This research used resources of (1) the GENCI-CINES/IDRIS (Grants c2011085117 and c2012085117), (2) CCIPL (Centre de Calcul Intensif des Pays de Loire), and (3) a local Troy cluster.

## ■ REFERENCES

(1) Mustroph, H.; Stollenwerk, M.; Bressau, V. *Angew. Chem., Int. Ed.* **2006**, *45*, 2016−2035.
(2) Cakmak, Y.; Akkaya, E. U. *Org. Lett.* **2009**, *11*, 85−88.
(3) Loudet, A.; Burgess, K. *Chem. Rev.* **2007**, *107*, 4891−4932.
(4) Zhang, Z.; Achilefu, S. *Chem. Commun.* **2005**, 5887−5889.
(5) Ulrich, G.; Ziessel, R.; Harriman, A. *Angew. Chem., Int. Ed.* **2008**, *47*, 1184−1201.
(6) Er, J.; Tang, M.; Chia, C.; H. Liew, M. V.; Chang, Y. *Chem. Sci.* **2013**, *4*, 2168−2176.
(7) Wang, X.; Weck, M. *Macromolecules* **2005**, *38*, 7219−7224.
(8) Cui, Y.; Wang, S. *J. Org. Chem.* **2006**, *71*, 6485−6496.
(9) Qin, Y.; Kiburu, I.; Shah, S.; Jakle, F. *Macromolecules* **2006**, *39*, 9041−9048.
(10) Qin, Y.; Kiburu, I.; Shah, S.; Jakle, F. *Org. Lett.* **2006**, *8*, 5227−5230.
(11) Nagata, Y.; Chujo, Y. *Macromolecules* **2007**, *40*, 6−8.
(12) Kaiser, P. F.; White, J. M.; Hutton, C. A. *J. Am. Chem. Soc.* **2008**, *130*, 16450−16451.
(13) Nagata, Y.; Otaka, H.; Chujo, Y. *Macromolecules* **2008**, *41*, 737−740.
(14) Feng, J.; Liang, B.; Wang, D.; Xue, L.; Li, X. *Org. Lett.* **2008**, *10*, 4437−4440.
(15) Zhou, Y.; Xiao, Y.; Chi, S.; Qian, X. *Org. Lett.* **2008**, *10*, 633−636.
(16) Bakalova, S.; Mendicuti, F.; Castano, O.; Kaneti, J. *Chem. Phys. Lett.* **2009**, *478*, 206−210.
(17) Tokoro, Y.; Nagai, A.; Chujo, Y. *Macromolecules* **2010**, *43*, 6229−6233.
(18) Zhou, Y.; Kim, J.; Kim, M.; Son, W.; Han, S.; Kim, H.; Han, S.; Kim, Y.; Lee, C.; Kim, S.; Kim, D.; Kim, J.; Yoon, J. *Org. Lett.* **2010**, *12*, 1272−1275.
(19) Frath, D.; Azizi, S.; Ulrich, G.; Retailleau, P.; Ziessel, R. *Org. Lett.* **2011**, *13*, 3414−3417.
(20) Yang, X.; Xia, M. *Acta Cryst. E* **2011**, *67*, o1049.
(21) Ma, R.; Yao, Q.; Yang, X.; Xia, M. *J. Fluor. Chem.* **2012**, *137*, 93−98.
(22) Massue, J.; Frath, D.; Ulrich, G.; Retailleau, P.; Ziessel, R. *Org. Lett.* **2012**, *14*, 230−233.
(23) Frath, D.; Azizi, S.; Ulrich, G.; Ziessel, R. *Org. Lett.* **2012**, *14*, 4774−4777.
(24) D'Aléo, A.; Gachet, D.; Heresanu, V.; Giorgi, M.; Fages, F. *Chem.—Eur. J.* **2012**, *18*, 12764−12772.
(25) Massue, J.; Frath, D.; Retailleau, P.; Ulrich, G.; Ziessel, R. *Chem.—Eur. J.* **2013**, *19*, 5275−5386.
(26) Massue, J.; Retailleau, P.; Ulrich, G.; Ziessel, R. *New J. Chem.* **2013**, *37*, 1224−1230.
(27) Chibani, S.; Le Guennic, B.; Charaf-Eddin, A.; Laurent, A. D.; Jacquemin, D. *Chem. Sci.* **2013**, *4*, 1950−1963.
(28) Le Guennic, B.; Chibani, S.; Charaf-Eddin, A.; Massue, J.; Ziessel, R.; Ulrich, G.; Jacquemin, D. *Phys. Chem. Chem. Phys.* **2013**, *15*, 7534−7540.
(29) Runge, E.; Gross, E. K. U. *Phys. Rev. Lett.* **1984**, *52*, 997−1000.
(30) Casida, M. E. In *Time-Dependent Density-Functional Response Theory for Molecules*; Chong, D. P., Ed.; Recent Advances in Density Functional Methods; World Scientific: Singapore, 1995; Vol. *1*; pp 155−192.
(31) Jacquemin, D.; Mennucci, B.; Adamo, C. *Phys. Chem. Chem. Phys.* **2011**, *13*, 16987−16998.
(32) More precisely, they have used the PBE0 hybrid functional and the 6-311+G(2d,p) atomic basis set.
(33) Santra, M.; Moon, H.; Park, M.; lee, T.; Kim, Y. K.; Ahn, K. H. *Chem.—Eur. J.* **2012**, *18*, 9886−9893.
(34) Singh, R. S.; Yadav, M.; Gupta, R. K.; Pandey, R.; Pandey, D. S. *Dalton Trans.* **2013**, *42*, 1696−1707.
(35) Laurent, A. D.; Jacquemin, D. *Int. J. Quantum Chem.* **2013**, DOI: 10.1002/qua.24438.
(36) Tozer, D. J. *J. Chem. Phys.* **2003**, *119*, 12697−12699.
(37) Dreuw, A.; Head-Gordon, M. *J. Am. Chem. Soc.* **2004**, *126*, 4007−4016.
(38) Masunov, A. E. *Int. J. Quantum Chem.* **2010**, *110*, 3095−3100.
(39) Le Guennic, B.; Maury, O.; Jacquemin, D. *Phys. Chem. Chem. Phys.* **2012**, *14*, 157−164.
(40) Jacquemin, D.; Zhao, Y.; Valero, R.; Adamo, C.; Ciofini, I.; Truhlar, D. G. *J. Chem. Theory Comput.* **2012**, *8*, 1255−1259.
(41) Improta, R.; Scalmani, G.; Frisch, M. J.; Barone, V. *J. Chem. Phys.* **2007**, *127*, 074504.
(42) Chibani, S.; Le Guennic, B.; Charaf-Eddin, A.; Maury, O.; Andraud, C.; Jacquemin, D. *J. Chem. Theory Comput.* **2012**, *8*, 3303−3313.
(43) Cossi, M.; Barone, V. *J. Chem. Phys.* **2001**, *115*, 4708−4717.
(44) Cammi, R.; Mennucci, B. *J. Chem. Phys.* **1999**, *110*, 9877−9886.
(45) Frisch, M. J.; Trucks, G. W.; Schlegel, H. B.; Scuseria, G. E.; Robb, M. A.; Cheeseman, J. R.; Scalmani, G.; Barone, V.; Mennucci, B.; Petersson, G. A.; Nakatsuji, H.; Caricato, M.; Li, X.; Hratchian, H. P.; Izmaylov, A. F.; Bloino, J.; Zheng, G.; Sonnenberg, J. L.; Hada, M.; Ehara, M.; Toyota, K.; Fukuda, R.; Hasegawa, J.; Ishida, M.; Nakajima, T.; Honda, Y.; Kitao, O.; Nakai, H.; Vreven, T.; Montgomery, J. A., Jr.; Peralta, J. E.; Ogliaro, F.; Bearpark, M.; Heyd, J. J.; Brothers, E.; Kudin, K. N.; Staroverov, V. N.; Kobayashi, R.; Normand, J.; Raghavachari, K.; Rendell, A.; Burant, J. C.; Iyengar, S. S.; Tomasi, J.; Cossi, M.; Rega, N.; Millam, J. M.; Klene, M.; Knox, J. E.; Cross, J. B.; Bakken, V.;

Adamo, C.; Jaramillo, J.; Gomperts, R.; Stratmann, R. E.; Yazyev, O.; Austin, A. J.; Cammi, R.; Pomelli, C.; Ochterski, J. W.; Martin, R. L.; Morokuma, K.; Zakrzewski, V. G.; Voth, G. A.; Salvador, P.; Dannenberg, J. J.; Dapprich, S.; Daniels, A. D.; Farkas, O.; Foresman, J. B.; Ortiz, J. V.; Cioslowski, J.; Fox, D. J. *Gaussian 09*, Revision C.01; Gaussian Inc.: Wallingford, CT, 2009.
(46) Stephens, P. J.; Devlin, F. J.; Chabalowski, C. F.; Frisch, M. J. *J. Phys. Chem.* **1994**, *98*, 11623−11627.
(47) Becke, A. D. *J. Chem. Phys.* **1993**, *98*, 5648−5652.
(48) Adamo, C.; Barone, V. *J. Chem. Phys.* **1999**, *110*, 6158−6170.
(49) Ernzerhof, M.; Scuseria, G. E. *J. Chem. Phys.* **1999**, *110*, 5029−5036.
(50) Zhao, Y.; Truhlar, D. G. *Theor. Chem. Acc.* **2008**, *120*, 215−241.
(51) Boese, A. D.; Martin, J. M. L. *J. Chem. Phys.* **2004**, *121*, 3405−3416.
(52) Yanai, T.; Tew, D. P.; Handy, N. C. *Chem. Phys. Lett.* **2004**, *393*, 51−56.
(53) Chai, J. D.; Head-Gordon, M. *Phys. Chem. Chem. Phys.* **2008**, *10*, 6615−6620.
(54) Chai, J. D.; Head-Gordon, M. *J. Chem. Phys.* **2008**, *128*, 084106.
(55) Tomasi, J.; Mennucci, B.; Cammi, R. *Chem. Rev.* **2005**, *105*, 2999−3094.
(56) Santoro, F.; Improta, R.; Lami, A.; Bloino, J.; Barone, V. *J. Chem. Phys.* **2007**, *126*, 084509.
(57) Santoro, F.; Improta, R.; Lami, A.; Bloino, J.; Barone, V. *J. Chem. Phys.* **2007**, *126*, 184102.
(58) Santoro, F.; Lami, A.; Improta, R.; Bloino, J.; Barone, V. *J. Chem. Phys.* **2008**, *128*, 224311.
(59) Valeur, B. *Molecular Fluorescence: Principles and Applications*; Wiley-VCH: Weinheim, 2002, pp 53.
(60) Avila Ferrer, F. J.; Cerezo, J.; Stendardo, E.; Improta, R.; Santoro, F. *J. Chem. Theory Comput.* **2013**, *9*, 2072−2082.
(61) The (//) notation indicates energy//geometry.
(62) Using the geometry optimized with the 6-31G(d) atomic basis set.
(63) Goerigk, L.; Grimme, S. *J. Chem. Phys.* **2010**, *132*, 184103.
(64) Jacquemin, D.; Planchat, A.; Adamo, C.; Mennucci, B. *J. Chem. Theory Comput.* **2012**, *8*, 2359−2372.
(65) Jacquemin, D.; Wathelet, V.; Perpète, E. A.; Adamo, C. *J. Chem. Theory Comput.* **2009**, *5*, 2420−2435.
(66) Le Bahers, T.; Adamo, C.; Ciofini, I. *J. Chem. Theory Comput.* **2011**, *7*, 2498−2506.
(67) Jacquemin, D.; Le Bahers, T.; Adamo, C.; Ciofini, I. *Phys. Chem. Chem. Phys.* **2012**, *14*, 5383−5388, Code available at Université de Nantes, http://www.sciences.univ-nantes.fr/CEISAM/erc/marches/ (accessed Aug. 6, 2012).